



HAL
open science

Thermal activation parameters of plastic flow reveal deformation mechanisms in the CrMnFeCoNi high-entropy alloy

G. Laplanche, J. Bonneville, C. Varvenne, W. A. Curtin, E. P. George

► **To cite this version:**

G. Laplanche, J. Bonneville, C. Varvenne, W. A. Curtin, E. P. George. Thermal activation parameters of plastic flow reveal deformation mechanisms in the CrMnFeCoNi high-entropy alloy. *Acta Materialia*, 2018, 143, pp.257-264. 10.1016/j.actamat.2017.10.014 . hal-01688044

HAL Id: hal-01688044

<https://hal.science/hal-01688044>

Submitted on 1 Jun 2023

HAL is a multi-disciplinary open access archive for the deposit and dissemination of scientific research documents, whether they are published or not. The documents may come from teaching and research institutions in France or abroad, or from public or private research centers.

L'archive ouverte pluridisciplinaire **HAL**, est destinée au dépôt et à la diffusion de documents scientifiques de niveau recherche, publiés ou non, émanant des établissements d'enseignement et de recherche français ou étrangers, des laboratoires publics ou privés.

This manuscript has been co-authored by UT-Battelle, LLC under Contract No. DE-AC05-00OR22725 with the U.S. Department of Energy. The United States Government retains and the publisher, by accepting the article for publication, acknowledges that the United States Government retains a non-exclusive, paid-up, irrevocable, world-wide license to publish or reproduce the published form of this manuscript, or allow others to do so, for United States Government purposes. The Department of Energy will provide public access to these results of federally sponsored research in accordance with the DOE Public Access Plan (<http://energy.gov/downloads/doe-public-access-plan>).

Thermal activation parameters of plastic flow reveal deformation mechanisms in the CrMnFeCoNi high-entropy alloy

G. Laplanche^{a*}, J. Bonneville^b, C. Varvenne^c, W.A. Curtin^d, E.P. George^{e,f}

^a Institut für Werkstoffe, Ruhr-Universität Bochum, D-44801 Bochum, Germany

^b Institut PPRIME, UPR 3346, University of Poitiers, CNRS, ENSMA, Dpt. of Physics and Mechanics of Materials, F-86962 Futuroscope Cedex, France

^c CINaM, UMR 7325, Aix-Marseille Univ. - CNRS, F-13288, Marseille, France

^d Institute of Mechanical Engineering, EPFL, Lausanne, CH-1015, Switzerland

^e Materials Science and Technology Division, Oak Ridge National Laboratory, Oak Ridge, Tennessee 37831-6115, USA

^f Department of Materials Science and Engineering, University of Tennessee, Knoxville, Tennessee 37996-2100, USA

*corresponding author: Tel.: +49 (0)234 32 25902

guillaume.laplanche@rub.de

Abstract

To reveal the operating mechanisms of plastic deformation in an FCC high-entropy alloy, the activation volumes in CrMnFeCoNi have been measured as a function of plastic strain and temperature between 77 K and 423 K using repeated load relaxation experiments. At the yield stress, σ_y , the activation volume varies from $\sim 60 b^3$ at 77 K to $\sim 360 b^3$ at 293 K and scales inversely with yield stress. With increasing plastic strain, the activation volume decreases and the trends follow the Cottrell-Stokes law, according to which the inverse activation volume should increase linearly with $\sigma - \sigma_y$ (Haasen plot). This is consistent with the notion that

hardening due to an increase in the density of forest dislocations is naturally associated with a decrease in the activation volume because the spacing between dislocations decreases. The values and trends in activation volume agree with theoretical predictions that treat the HEA as a high-concentration solid-solution-strengthened alloy. These results demonstrate that this HEA deforms by the mechanisms typical of solute strengthening in FCC alloys, and thus indicate that the high compositional/structural complexity does not introduce any new intrinsic deformation mechanisms.

Keywords: High-entropy Alloys; CoCrFeMnNi Plastic deformation mechanisms; Stress relaxation; Dislocations; Activation volume

1. Introduction

Plastic deformation of metals and alloys is observed to be temperature and strain rate dependent, indicating that the motion of dislocations is controlled by thermally activated processes in the metal. The thermally activated process(es) are governed by the stress-dependent Gibbs free energy $\Delta G(\sigma)$ that captures the energies required for a gliding dislocation to overcome/bypass various metallurgical obstacles (such as solute atoms, precipitates, forest dislocations, sessile locks) in the alloy. The temperature dependence of the plastic strain rate $\dot{\epsilon}$ is usually expressed by an Arrhenius-type equation [1].

$$\dot{\epsilon} = \dot{\epsilon}_0 \exp\left(\frac{-\Delta G(\sigma)}{kT}\right),$$

(1)

where k is the Boltzmann's constant, T the absolute temperature, and $\dot{\epsilon}_0$ a microstructure-dependent rate parameter.

Because the various possible obstacles span a wide range of physical scales, it is the activation volume V that reveals the operative size scale in the material at temperature T , plastic strain rate $\dot{\epsilon}$, and stress σ . The activation volume represents the volume of matter involved in the thermally activated processes driven by a resolved shear stress τ acting on coherent thermal fluctuations of dislocation segments, and is defined as

$$V = \frac{-\partial(\Delta G(\tau))}{\partial \tau} \Big|_T = -M \frac{\partial \ln(\dot{\epsilon})}{\partial \sigma} \Big|_T = M k T \frac{\partial \ln(\dot{\epsilon})}{\partial \sigma} \Big|_T = b A \quad (2)$$

where $M = 3.06$ is the Taylor factor that relates the uniaxial stress σ and resolved shear stress τ in an equiaxed polycrystal, b is the magnitude of the Burgers vector of a perfect dislocation, and A is the activation area swept by the dislocation in reaching the activated state. Commonly, activation volumes are expressed in units of b^3 : for instance, individual point defects provide activation volumes on the order of b^3 , forest dislocations provide activation volumes on the order of $V \sim b w l$ where $l = 1/\sqrt{\rho} \gg b$ is the forest spacing for a dislocation density of ρ , and $w > b$ characterizes the local junction energetics, while collective solute fluctuations in dilute solid solutions yield $V \sim 1000 b^3$ [1-12]. For reference, $b = 0.255$ nm in our CrMnFeCoNi alloy [13], so $b^3 \sim 0.017$ nm³. The activation volume is thus a very useful measure for uncovering the underlying length scales of the thermally-activated process(es) of plastic flow, which then points toward the specific operating mechanism(s) in the material.

High-entropy alloys (HEAs) are an emerging new class of materials with the potential for impressive properties [14-31]. Some HEAs exhibit good yield and high ultimate tensile

strengths, high ductility, excellent fracture toughness, and retain strength at elevated temperatures. The large number of possible compositions and classes of HEAs have led to the creation of many different systems, and the origins of their mechanical properties have been the subject of considerable discussion, as researchers draw on the wide range of mechanisms known in established alloys and propose new concepts.

To provide deeper insight into the mechanisms of plastic deformation, we measure the activation volume versus temperature and plastic strain in the well-established and widely studied FCC equiatomic alloy CrMnFeCoNi [32] in the solid solution state. Trends in the activation volume are interpreted within the context of theory and reveal that the mechanisms of rate-dependent deformation are solid-solution strengthening and forest hardening. The recent theory for initial yield strength of HEAs based on solid-solution strengthening is shown to provide some quantitative agreement with the initial activation volume at the initial yield stress as a function of temperature. Thus the findings here support the notion that the deformation mechanisms in FCC HEAs are precisely those found in dilute solid-solution alloys [33-42]. The additional complexity of compositional disorder in this HEA appears not to play a direct role in establishing the material strengthening and rate dependence.

The remainder of this paper is organized as follows. In Section 2, we describe the experimental methods and analysis used to obtain the activation volume. In Section 3, we summarize a specific theoretical framework for flow stress versus strain rate, temperature, and plastic strain. In Section 4, we present our results and compare to theoretical predictions (qualitatively and quantitatively). Section 5 contains further discussion and a brief summary.

2. Experimental methods and analysis

2.1 Material

An equiatomic CrMnFeCoNi HEA was vacuum induction melted, homogenized, swaged and recrystallized at 900°C for 1 h. Previously, this process was shown to produce material that is single-phase, FCC, nearly untextured, and with a mean grain size $d \sim 17 \mu\text{m}$ [43]. The grains are equiaxed and contain annealing twins whose density was determined to be 2.3 ± 0.1 twins per grain using the procedure used in Ref. [44].

2.2 Mechanical tests

After recrystallization, rectangular dog-bone shaped tensile samples (gauge length: 20 mm) were machined by electrical discharge machining with their loading axes parallel to the axis of the swaged rod. They were then ground to 1000 grit finish using SiC paper resulting in a final thickness and gauge width of ~ 1.2 mm and ~ 4 mm, respectively. Tensile tests were performed at engineering strain rates of 10^{-5} s^{-1} and 10^{-3} s^{-1} in a screw-driven Zwick/Roell test rig of type Z100 in the temperature range [77 K - 423 K]. During the tests performed at 77 K, the specimens and grips were kept fully immersed in liquid nitrogen. The higher temperature tests were performed in a temperature-controlled chamber. Activation parameters were determined using repeated load relaxation tests [45] at various plastic strains as follows. After starting the tensile tests at an engineering strain rate of either 10^{-5} s^{-1} or 10^{-3} s^{-1} , when the desired plastic strain was reached, the cross-head was stopped abruptly for 30 s and the load recorded as a function of time (Fig. 1). Then the specimen was re-loaded to the stress at which the first load relaxation started and the next load relaxation was started. This process was repeated four times to give a total of five load relaxations in each set. The magnified inset in Fig. 1 shows two such load relaxation sets performed at comparable flow stresses (~ 407 - 410 MPa) at strain rates of 10^{-3} s^{-1} (red curve) and 10^{-5} s^{-1} (black curve). As the activation volumes determined at 293 K for strain rates of 10^{-5} s^{-1} and 10^{-3} s^{-1} were found to be

similar (within $\pm 5\%$), it was concluded that strain rate (in this range) does not affect the activation volume and all subsequent experiments were performed at a strain rate of 10^{-3} s^{-1} .

2.3 Experimental determination of activation volumes

The apparent activation volumes (V_{app}) are obtained by fitting the following logarithmic relationship to the first relaxation curve of the repeated load relaxation tests [46]:

$$\Delta\sigma = \frac{-MkT}{V_{app}} \ln\left(1 + \frac{t}{c}\right), \quad (3)$$

where $\Delta\sigma < 0$ is the stress decrease during the relaxation time t , the constant

$$c = \frac{\dot{\epsilon}_p^0}{V_{app} S \dot{\epsilon}_p^0}, \quad S \text{ is the elastic modulus of the machine-specimen assembly, and}$$

$\dot{\epsilon}_p^0$ is the plastic strain rate at the start of the load relaxation test. Equation (3) is obtained from a first order Taylor expansion of $\Delta G(\sigma)$ with respect to the flow stress, i.e., the apparent activation volume is assumed to be constant during the load relaxation test. As a consequence, when activation volumes are stress dependent (as they usually are), load relaxations must be analyzed over a “short duration” during which the activation volume can be considered to be constant so that the above Taylor expansion of $\Delta G(\sigma)$ remains valid [47].

Physical activation volumes V are related to apparent activation volumes V_{app} by the following equation [48]

$$V_{app} = V \left(1 + \frac{\Theta}{S}\right), \quad (4)$$

where Θ is the work-hardening rate ($d\sigma/d\varepsilon$) and S is the elastic modulus of the machine-specimen assembly, encountered before **in the expression of c in Eq. (3)**. Therefore, apparent activation volumes have to be corrected to account for the effects of work hardening of the specimen as well as the stiffness of the test rig. In general, the correction cannot be ignored unless the testing machine is very rigid and/or the specimen does not work harden significantly. While apparent activation volumes are determined from the first load relaxation, subsequent load relaxations allow us to determine $V \times \Theta/S$ following Spätig et al. [45] who showed that $V_{app} - V = V \times \Theta/S$ is related to the successive stress drops in repeated load relaxation tests:

$$(n-1)V \frac{\Theta}{S} = \frac{M k T}{\Delta \bar{\sigma}} \ln \left(\frac{\exp\left(\frac{-\Delta \sigma_n V_{app}}{M k T}\right) - 1}{\exp\left(\frac{-\Delta \sigma_1 V_{app}}{M k T}\right) - 1} \right), \quad (5)$$

where n is the number of load relaxations, $\Delta \sigma_1$ and $\Delta \sigma_n$ are the stress drops in the first and n^{th} load relaxation, respectively, and the average stress drop is given by

$$\Delta \bar{\sigma} = \frac{1}{n} \sum_n \Delta \sigma_n . \quad (6)$$

Therefore, a plot of the right-hand side of Eq. (5) versus n yields a straight line, with a slope equal to $V \times \Theta/S$. Note that, in some cases, Θ can also include a term that accounts for the variation in the density of mobile dislocations during the load relaxation [49].

3. Theory of activation volume in solute-strengthened FCC alloys

3.1 General framework

As a framework for interpreting the experimental results, we envision that the strength of the FCC HEA behaves similarly to the many solute-strengthened FCC alloys studied over many decades, but usually in the dilute limit. The strengthening in such systems consists mainly of three contributions: (i) a grain-size-dependent Hall-Petch strengthening (σ_{HP} with length scale d), (ii) solid solution strengthening in the random alloy (σ_{ss} with length scale $\zeta_c \sim 10$ nm), and (iii) dislocation-dislocation interactions in the form of forest hardening (σ_f with length scale l). For the sake of simplicity, we ignore in our analysis other dislocation obstacles such as sessile locks and, for the monotonic loading tests performed here, it is not necessary to characterize the hardening in terms of macroscopic continuum concepts such as the isotropic and kinematic hardening components. When multiple mechanisms operate at very different scales, as is the case here with $d \gg l \gg \zeta_c$, it is common to assume that the strengthening contributions are additive. We can thus write the alloy strength in the form

$$\sigma(T, \dot{\epsilon}, \epsilon_p, d) = \sigma_{\text{HP}}(d) + \sigma_{\text{ss}}(T, \dot{\epsilon}) + \sigma_f(T, \dot{\epsilon}, \epsilon_p) \quad , \quad (7)$$

where the Hall-Petch strengthening $\sigma_{\text{HP}}(d)$ is usually found to be athermal (rate- and temperature-independent) [16, 50] and independent of plastic strain [51], the solute strengthening $\sigma_{\text{ss}}(T, \dot{\epsilon})$ is temperature and strain rate dependent, and the forest hardening $\sigma_f(T, \dot{\epsilon}, \epsilon_p)$ has an additional dependence on total plastic strain due to

evolution/multiplication of dislocation density. When the strengths are additive, the activation volume of Eq. (2) can be derived as

$$\frac{1}{V} = \frac{1}{M k T} \frac{\partial \sigma}{\partial \ln(\dot{\epsilon})} = \frac{1}{M k T} \frac{\partial \sigma_{ss}}{\partial \ln(\dot{\epsilon})} + \frac{1}{M k T} \frac{\partial \sigma_f}{\partial \ln(\dot{\epsilon})} = \frac{1}{V_{ss}} + \frac{1}{V_f} .$$

(8)

The Hall-Petch mechanism does not contribute to the activation volume, while the inverse activation volumes of the two rate-dependent strengthening mechanisms are additive, i.e., solute strengthening and forest hardening.

3.2 Forest hardening

The strengthening due to forest hardening is $\sigma_f = M \alpha \mu b \sqrt{\rho}$ where the parameter $\alpha = \alpha(T, \dot{\epsilon})$ reflects, in principle, the rate dependency associated with the breaking of dislocation junctions in the forest network and μ is the shear modulus. The activation volume for forest hardening is associated with the area swept out by the dislocation over length $l = 1/\sqrt{\rho}$ combined with overcoming the junction barrier over some length scale w , $V \sim b w l$. The length scale $w(\tau)$ varies with the resolved shear stress τ , in principle, but this is usually neglected as small compared to the dependence of V on l (and hence on σ). The exact origin of thermal activation is believed in the literature to be related to the formation of jogs on intersecting dislocations or the recombination of short attractive junctions [52, 53]. The activation volume for forest hardening can thus be written as

$$V_f \sim w M \alpha \mu b^2 / \sigma_f .$$

(9)

The inverse activation volume for forest hardening thus scales linearly with forest hardening,

$$\frac{1}{V_f} \sim \beta \frac{\sigma_f}{M} , \quad (10)$$

where β is a combination of material parameters. Eq. (10) is the long-established Cottrell-Stokes law observed in pure elemental FCC metals.

3.3 Solute strengthening

A general theory for solute strengthening of random FCC alloys at dilute solute concentrations has recently been developed [35, 36, 40]. A dislocation in the random alloy responds to the presence of spatially-varying solute concentrations by adopting a wavy shape characterized by wavelength $2\zeta_c$ and amplitude w_c . The characteristic waviness (ζ_c, w_c) is that which minimizes the total dislocation energy by enabling the dislocation to reside in regions of favorable (energy-lowering) regions of solute concentration fluctuations at the expense of the line tension cost of the wavy shape. The inputs to the theory are the solute/dislocation interaction energies in the alloy, the dislocation line tension Γ , the dislocation Burgers vector b , and alloy composition. The outcomes of the theory are a zero-temperature yield stress τ_{y0} and activation energy barrier ΔE_b . These combine to give the activation free energy ΔG as

$$\Delta G = \Delta E_b(T) \left(1 - \frac{\tau}{\tau_{y0}(T)} \right)^{3/2} \text{ for } \tau > 0.5\tau_{y0}(T) , \quad (11)$$

$$\Delta G = 0.55 \Delta E_b(T) \ln\left(\frac{\tau_{y0}(T)}{\tau}\right) \text{ for } \tau < 0.5 \tau_{y0}(T), \quad (12)$$

where $\Delta E_b(T) = \frac{\mu(T)}{\mu(0)} \Delta E_b$ and $\tau_{y0}(T) = \frac{\mu(T)}{\mu(0)} \tau_{y0}$ are the *apparent* zero-temperature flow stress and activation barrier accounting for the change in the alloy's shear modulus μ at finite temperature T . The transition in form with decreasing τ is discussed fully in Ref. [38], and the second form, Eq. (12), is necessary to capture behavior at high temperatures (lower stresses). In fact, the difference between the two equations is small around $\tau = 0.5 \tau_{y0}(T)$.

The finite-temperature/finite-strain rate flow stress then follows directly from application of the Arrhenius law of Eq. (1) as

$$\sigma_{ss}(T, \dot{\epsilon}) = M \tau_{y0}(T) \left[1 - \left(\frac{kT}{\Delta E_b(T)} \ln\left(\frac{\dot{\epsilon}_0}{\dot{\epsilon}}\right) \right)^{2/3} \right] \text{ for } \sigma_{ss}(T) > 0.5 \sigma_{y0}(T), \quad (13)$$

$$\sigma_{ss}(T, \dot{\epsilon}) = M \tau_{y0}(T) \exp\left(\frac{-kT}{0.55 \Delta E_b(T)} \ln\left(\frac{\dot{\epsilon}_0}{\dot{\epsilon}}\right)\right) \text{ for } \sigma_{ss}(T) < 0.5 \sigma_{y0}(T). \quad (14)$$

The activation volume for solid solution strengthening is then also obtained directly from ΔG using Eq. (2) as

$$V_{ss}(T, \dot{\epsilon}) = \frac{3 \Delta E_b(T)}{2 \tau_{y0}(T)} \left(\frac{kT}{\Delta E_b(T)} \ln\left(\frac{\dot{\epsilon}_0}{\dot{\epsilon}}\right) \right)^{1/3} \text{ for } \sigma_{ss}(T) > 0.5 \sigma_{y0}(T) \quad (15)$$

$$V_{ss}(T, \dot{\epsilon}) = \frac{0.55 \Delta E_b(T)}{\tau_{y0}(T)} \exp\left(\frac{k T}{0.55 \Delta E_b(T)} \ln\left(\frac{\dot{\epsilon}_0}{\dot{\epsilon}}\right)\right) = \frac{0.55 M \Delta E_b(T)}{\sigma_{ss}(T, \dot{\epsilon})} \quad \text{for } \sigma_{ss}(T) < 0.5 \sigma_{y0}(T)$$

(16)

The physical underlying scale for the activation volume due to solid solution strengthening is $\Delta E_b / \tau_{y0} \sim b w_c \zeta_c$. The measured activation volume thus directly reveals the product of the key length scales of the wavy dislocation in the solute-strengthened random alloy. In dilute alloys, the predictions of the activation volume versus yield strength, temperature, and/or solute concentration follow experimental trends, and quantitatively are within a factor of 2 [38, 40].

The “dilute limit” model has been extended to arbitrary compositions, making it applicable to HEAs [39]. The underlying concept is that the complex alloy can be viewed as an “effective” matrix that reflects the average properties of the alloy (lattice constant, elastic constants, stacking fault energy, line tension) into which all alloy elements are added as solutes. Each alloy solute n has a well-defined misfit volume ΔV_n in the “effective” matrix material and, more generally, a well-defined interaction energy with a dislocation in the “effective” matrix material. The use of the “effective” matrix accounts for the average surrounding atomic environments that any one solute atom would experience in the alloy. The full interaction energy includes misfit volume, stacking fault energy, core interactions, and the explicit consideration of local spatial fluctuations of the solutes then includes local variations in stacking fault energy. The reduced elasticity theory neglects stacking fault energies, but also shows that the predicted strength is essentially independent of partial dislocation spacing.

The full theory can be reduced to an analytic model by assuming that the solute/dislocation interaction energies are due only to the elastic interaction between the

solute misfit volume and the pressure field of the dislocation in the effective alloy matrix. For alloys with a partial dislocation separation larger than $\sim 10 b$, the partial dislocation separation does not influence the low-to-intermediate temperature results [40]. This rationalizes the observations of variations in stacking fault width [41] because the two partial dislocations adjust their positions, around the average spacing dictated by the average stacking fault energy and elastic interactions, in response to their local solute fluctuations. The model has been applied with quantitative success to the Cr-Mn-Fe-Co-Ni family [39]. For the Cantor alloy studied here, the key alloy properties are computed to be

$$\tau_{y0} = 83 \text{ MPa}; \quad \Delta E_b = 1.13 \text{ eV},$$

(17)

where the line tension has been expressed as $\Gamma = \gamma \mu b^2$ with the value $\gamma = 0.123$ measured in several molecular statics simulations of FCC metals. For comparison purposes, results for a smaller line tension parameter $\gamma = 0.06125$ yield

$$\tau_{y0} = 104 \text{ MPa}; \quad \Delta E_b = 0.905 \text{ eV}.$$

(18)

The temperature-dependent parameters $\tau_{y0}(T)$ and $\Delta E_b(T)$ then follow by rescaling with the measured finite-temperature shear moduli $\frac{\mu(T)}{\mu(0)}$. This theory thus makes specific parameter-free predictions for the contributions of solid solution alloying to both the initial yield stress and activation volume via Eqs. 13-16.

3.4 Activation volume in solute-strengthened FCC alloys

Combining the contributions of forest hardening and solid solution strengthening to the overall activation volume of the alloy, the above theory (using the high-T/low-stress form for the solid solution strengthening, for simplicity) predicts

$$\frac{1}{V} = \frac{1}{V_{ss}} + \frac{1}{V_f} = \frac{1}{0.55 \Delta E_b(T) M} \sigma_{ss}(T, \dot{\epsilon}) + \beta \frac{\sigma_f(\epsilon_p)}{M} . \quad (19)$$

The first term is independent of plastic strain while the second term increases with plastic strain due to dislocation multiplication that leads to the forest hardening. The inverse activation volume is then typically expressed in terms of the applied stress using Eqs. (7) and (19) as

$$\frac{1}{V} = \frac{1}{0.55 \Delta E_b(T) M} \sigma_{ss}(T, \dot{\epsilon}) + \frac{\beta}{M} (\sigma - \sigma_y) \text{ with } \sigma_y = \sigma_{HP}(d) + \sigma_{ss}(T, \dot{\epsilon}) , \quad (20)$$

where σ_y is the initial yield stress. This form corresponds to the well-established Haasen plot, $1/V$ versus $\sigma - \sigma_y$, with the intercept value associated solely with solute strengthening and the slope associated solely with forest hardening.

4. Results and discussion

4.1 Tensile tests

Fig. 1 shows stress-strain curves obtained at 293 K for strain rates of 10^{-3} s^{-1} (red curve) and 10^{-5} s^{-1} (black curve). The two stress-strain curves are remarkably similar indicating that strain rate (in this range) has a small effect on the flow stress behavior. These results are consistent with earlier results [15] that showed the relative insensitivity of the yield and ultimate tensile strengths of this alloy to strain rate in this range. This will be discussed further in Section 4.2 in terms of the strain rate sensitivity of stress.

True stress-strain curves obtained in the temperature range [77 K – 423 K] are shown in Fig. 2 where several repeated load relaxations at various plastic strains can be observed. Except for the tensile test performed at 293 K, which was unloaded after ~20% plastic strain, all other tests were taken to fracture/necking. Fig. 2 reveals that, for a given strain, the flow stress and the work-hardening rate increase with decreasing temperature. Consistent with the Considère criterion, $d\sigma/d\varepsilon = \sigma$, the increased work hardening rate at lower temperatures postpones necking, resulting in the ductility increasing with decreasing temperature. These results are in good agreement with those reported in earlier studies of the CrMnFeCoNi HEA [15, 16, 18, 29].

Fig. 3 presents the yield stress at 0.2 % plastic strain (black data points) as a function of temperature, showing a strong decrease of yield stress with increasing temperature. The Hall-Petch parameters reported by Otto et al. [16] were used to extrapolate the results at $d = 17 \text{ }\mu\text{m}$ to infinite grain size (blue data points), thereby revealing the intrinsic lattice strength. The temperature dependence of the shear modulus is weak, reported previously to decrease from 85 GPa at 77 K [54] to 75 GPa at 423 K [55], that is by ~12%. Therefore, the much larger decrease of the initial yield strength (~70%) over the same temperature range cannot be due simply to softening of the shear modulus; rather it must reflect thermally-activated processes. Although small, note that the temperature dependence of the elastic

constants is included in the theoretical strength predictions discussed earlier (see Eqs. 13 and 14).

Fig. 3 also shows the temperature dependence of yield stress calculated using Eqs. (14, 17, 18), the two values of τ_{y0} and ΔE_b (for $\gamma = 0.123$, green, and 0.0625, red), and a reference strain rate of $\dot{\epsilon}_0 = 10^4/s$, consistent with previous work [39]. The theory underpredicts the strength at 77 K but otherwise is in generally good agreement with experiments, including previous yield strengths [16] that are 10 MPa lower than the present results at 293 K (which are within typical experimental uncertainties of ± 10 MPa). The predictions at 77 K are particularly sensitive to the line tension parameter, but remain below experiments nonetheless. Possible rationale for this difference is discussed in [39]. Overall, the solid solution strengthening model captures, both qualitatively and quantitatively, the main features of the initial yield stress versus temperature.

4.2 Repeated load relaxation tests

Repeated load relaxation experiments were performed at various plastic strains and it was found that the activation volume decreased with true plastic strain, see Fig. 4. Recent TEM studies have shown that the CrMnFeCoNi HEA exhibits a very low dislocation density in the recrystallized state, which rapidly increases with plastic strain [13, 16]. Since the dislocation density is low in the initial state ($\rho = 3.2 \times 10^{12} \text{ m}^{-2}$ [13]), the activation volume at initial yielding presumably reflects the interaction of dislocations with solutes. Upon straining to $\sim 17.5\%$ true plastic strain (both at 293 K and 77 K), the dislocation density increases, which corresponds to a decrease in the dislocation spacing ($l = 1/\sqrt{\rho}$). Consistent with this reasoning, Fig. 4 shows a decrease of activation volume with strain. The experimental trends are consistent with the general theoretical framework of Section 3.

Further analysis of these trends is possible by plotting the quantity $M k T/V$ versus the offset flow stress $\sigma - \sigma_y$, in the form of the so-called Haasen plot, as shown in Fig. 5. For materials strengthened by a combination of Hall-Petch strengthening, solute strengthening, and forest hardening, the positive intercept of the Haasen plot is conventionally associated with solute strengthening and its slope with forest hardening. In Fig. 5, neither the intercept values nor the slopes have any clear trend with temperature, consistent with the expectations of the general model. Therefore, the present experimental results are fully consistent with a “standard” interpretation of the thermally activated flow of solute-strengthened metal alloys.

In another study, it was shown that CrMnFeCoNi with the same grain size as here ($d = 17 \mu\text{m}$) deforms by dislocation plasticity at applied stresses below 720 MPa (athermal critical twinning stress) while at higher stresses both deformation twinning and dislocation plasticity are active [13]. In Fig. 5, it can be seen that the activation volume V is inversely proportional to forest hardening, $\sigma - \sigma_y$, below and above the twinning stress (e.g., at 77 K, the twinning stress is reached when $\sigma - \sigma_y = 270 \text{ MPa}$ and there is no visible discontinuity there). It can therefore be concluded that deformation twinning does not have an influence on the evolution of activation volumes with flow stress. This conclusion is in good agreement with that of Hong et al. [56] who suggested that twinning does not have any significant influence on activation volumes. This is not too surprising since the spacing between deformation twins was found to be much larger than the spacing between dislocations, e.g., after 16% plastic strain at 77 K, the mean twin spacing is $\sim 5 \mu\text{m}$ while the spacing between dislocations is $\sim 0.06 \mu\text{m}$ [13].

Proceeding next to a more quantitative comparison between our experimental results and the theory developed in Section 3, Fig. 6 shows the temperature dependence of V (in units of b^3) obtained at the yield stress, from experiments (black data points) and theory (for γ

= 0.123 and 0.0625 in green and red colors, respectively). The theory predicts the general magnitude of the activation volumes, $V \sim 100 b^3$, and the trend of increasing activation volume with increasing temperature. Quantitatively, the predicted activation volumes are generally smaller than the experimental values, especially with increasing temperature, but remain within a factor of 1-3 throughout the range of temperatures studied here. As with the initial yield strength predictions, the activation volumes predicted using the line tension parameter $\gamma = 0.0625$ (red data points) show a trend closer to the experimental trend, but with smaller magnitude than the values obtained with $\gamma = 0.123$ (green data points). Overall, the level of agreement here is comparable to that achieved in dilute FCC alloys, including comparisons that simply use fitted values of τ_{y0} and ΔE_b , and so better agreement should not be anticipated.

To put our present results in context, we will now address two recent studies of activation volumes in CrMnFeCoNi that we believe were incorrectly performed and interpreted. Wu et al. [57] determined activation volumes by means of strain rate jumps at engineering plastic strains of 5%, 15%, and 25% at 293 K and 77 K. Since the measurements were made at strains of 5% or more, their activation volumes cannot reflect only solid solution effects as claimed, since the contribution of forest hardening to the activation volume is important (see Eq. (8) and Fig. 4) and has to be included. Therefore, the activation volumes reported by Wu et al. [57] are likely underestimates and the strain rate sensitivity of stress overestimates. Moreover, in their expression for the activation volume, Eqs. (6) and (7) in Ref. [57], there is a $\sqrt{3}$ -factor, which Wu et al. [57] introduced for the conversion between normal and shear stresses. This is an error because they should have used the Taylor factor ($M = 3.06$) to convert polycrystalline yield stress to critical resolved shear stress (after accounting for Hall-Petch) as is done in our present study. It appears from their $\sqrt{3}$ -factor,

although we cannot be certain, that Wu et al. mistakenly used the von Mises yield criterion for multiaxial loading, which would be inappropriate given that they performed uniaxial tensile tests. This results in an additional underestimation by a factor 1.7 of the activation volumes. Furthermore, in some of the stress-strain curves shown in Wu et al. [57], the x-axis is labelled as "plastic strain" when it clearly shows the elastic portion too. From their description, it is not clear whether they used true values of stress and strain in their analyses or just engineering values (which would be inappropriate). Perhaps the biggest problem in Wu et al. [57] is their finding that activation volumes are independent of plastic strain. This is contrary to what has been traditionally observed in pure FCC metals, dilute and concentrated solid solutions, as well as, more recently, in HEAs [9, 10, 58-63]. It is also not physically reasonable given that the governing length scale (spacing between the dislocation trees in the forest) decreases with increasing strain and, therefore, casts doubt on the validity of the activation volumes reported by Wu et al [57].

In a more recent study, Hong et al. [56] measured activation volumes in the same alloy at different plastic strains by strain rate jumps from 10^{-3} to 10^{-2} s⁻¹. The authors reported that activation volumes increase with increasing plastic strain, which is contrary to what is usually observed in FCC solid solutions as discussed above, i.e., activation volumes decrease with plastic strain as a result of forest hardening. In Fig. 3 of Hong et al. [56], it can be clearly seen that the tensile stress-strain curves are rather noisy, relative to which the magnitude of the stress change induced by the strain rate jumps is small. This is because they changed strain rate by only an order of magnitude, as opposed to at least a two orders of magnitude jump needed to reliably characterize FCC metals. As a consequence, the uncertainty in their

activation volumes is probably as large as the activation volume itself and their measurements are not accurate enough to capture the real evolution of activation volume with plastic strain.

Another parameter commonly used to describe thermally activated flow behavior is the strain rate sensitivity (m) defined as [3, 7, 64]

$$m = \frac{\partial \ln(\sigma)}{\partial \ln(\dot{\epsilon}_p)} = \frac{1}{\sigma} \frac{\partial \sigma}{\partial \ln(\dot{\epsilon}_p)} = \frac{M k T}{V \sigma} \quad . \quad (21)$$

Since the Haasen plot shows that $\frac{M k T}{V} = \frac{1}{0.55 \Delta E_b} \sigma_{ss}(T, \dot{\epsilon}) + \frac{\beta}{M} (\sigma - \sigma_{HP} - \sigma_{ss}(T, \dot{\epsilon}))$, m is expected to have no special form in terms of σ . However, due to competing effects of the material parameters $\Delta E_b, \sigma_{ss}(T, \dot{\epsilon}), \beta$, and σ_{HP} , computation of m using the experimental data leads to a nearly constant value of $m = 0.0073 \pm 0.0009$ across all temperatures and stresses, with a slight general trend of decreasing m with increasing flow stress. The small value of m is consistent with the macroscopic insensitivity of the flow stress to strain rate, with a change in plastic strain rate from 10^{-5} s^{-1} to 10^{-3} s^{-1} resulting in a relative increase of the flow stress of $\sim 3.4\%$ (at initial yield $\Delta \sigma_y \approx 9 \text{ MPa}$). This value is of the same order of magnitude as the standard deviation ($\sim 10 \text{ MPa}$) of the yield stress as determined from tensile tests of more than 14 specimens at 293 K and a strain rate of 10^{-3} s^{-1} [13]. Therefore, it is difficult to extract the change in yield stress due to a change in plastic strain rate from 10^{-5} s^{-1} to 10^{-3} s^{-1} given the scatter in the stress-strain curves. This can be seen from the two representative stress-strain curves shown in Fig. 1 where, despite the two orders of magnitude difference in strain rate, there is little difference in the flow behaviors.

5. Summary and conclusion

The activation volume in the Cantor alloy CrMnFeCoNi has been measured as a function of temperature using load relaxation tests. The results have been interpreted within a standard framework for solid-solution-strengthened FCC alloys, and the experimental trends conform to this standard framework. This finding indicates that plastic flow in this alloy is controlled by a combination of (i) rate-independent Hall-Petch strengthening, (ii) thermally activated solid solution strengthening, and (iii) forest hardening that evolves with plastic strain. The thermally activated solid solution strengthening component has been compared to a recent theory for HEAs, and good agreement in magnitude and trends is found, to a level similar to that obtained in standard dilute solid solution alloys. Therefore, we conclude that the dominant deformation mechanisms controlling rate-dependent flow in this HEA material are the same as those found in other FCC alloys; no new mechanisms need to be invoked in spite of the high atomic-scale complexity of the material.

Acknowledgments

GL acknowledges funding from the German Research Foundation (Deutsche Forschungsgemeinschaft DFG) through project LA 3607/1-1. JB also thanks the DFG for financial support during his stay at the Ruhr University Bochum. WAC acknowledges support from a European Research Council Advanced Grant, “Predictive Computational Metallurgy”, ERC Grant agreement No. 339081 - PreCoMet. EPG is sponsored by the U.S. Department of Energy, Office of Science, Basic Energy Sciences, Materials Sciences and Engineering Division.

References

- [1] G. Schoeck, The Activation Energy of Dislocation Movement, *Physica Status Solidi* 8 (1965) 499.
- [2] A.H. Cottrell, R.J. Stokes, Effects of Temperature on the Plastic Properties of Aluminium Crystals, *Proceedings of the Royal Society of London A: Mathematical, Physical and Engineering Sciences* 233 (1955) 17.
- [3] P. Haasen, Plastic deformation of nickel single crystals at low temperatures, *Philosophical Magazine* 3 (1958) 384.
- [4] Z. Basinski, Thermally activated glide in face-centred cubic metals and its application to the theory of strain hardening, *Philosophical Magazine* 4 (1959) 393.
- [5] A.G. Evans, R.D. Rawlings, The thermally activated deformation of crystalline materials, *physica status solidi (b)* 34 (1969) 9.
- [6] L. Brown, R. Ham, Strengthening methods in crystals, *Applied Science, London* 9 (1971).
- [7] U.F. Kocks, Thermodynamics and kinetics of slip, *Progress in Material Science* 19 (1975) 1.
- [8] R. Mulford, U. Kocks, New observations on the mechanisms of dynamic strain aging and of jerky flow, *Acta Metallurgica* 27 (1979) 1125.
- [9] B. Diak, S. Saimoto, The determination of solute clusters in dilute aluminum alloys using strain rate sensitivity, *Materials Science and Engineering: A* 234 (1997) 1019.
- [10] B. Diak, K. Upadhyaya, S. Saimoto, Characterization of thermodynamic response by materials testing, *Progress in materials science* 43 (1998) 223.
- [11] A. Argon, *Strengthening mechanisms in crystal plasticity*, Oxford University Press on Demand, 2008.
- [12] G. Laplanche, J. Bonneville, A. Joulain, V. Gauthier-Brunet, S. Dubois, Mechanical properties of Al-Cu-Fe quasicrystalline and crystalline phases: An analogy, *Intermetallics* 50 (2014) 54.
- [13] G. Laplanche, A. Kostka, O.M. Horst, G. Eggeler, E.P. George, Microstructure evolution and critical stress for twinning in the CrMnFeCoNi high-entropy alloy, *Acta Materialia* 118 (2016) 152.
- [14] O.N. Senkov, G.B. Wilks, J.M. Scott, D.B. Miracle, Mechanical properties of $\text{Nb}_{25}\text{Mo}_{25}\text{Ta}_{25}\text{W}_{25}$ and $\text{V}_{20}\text{Nb}_{20}\text{Mo}_{20}\text{Ta}_{20}\text{W}_{20}$ refractory high entropy alloys, *Intermetallics* 19 (2011) 698.
- [15] A. Gali, E.P. George, Tensile properties of high- and medium-entropy alloys, *Intermetallics* 39 (2013) 74.
- [16] F. Otto, A. Dlouhý, C. Somsen, H. Bei, G. Eggeler, E.P. George, The influences of temperature and microstructure on the tensile properties of a CoCrFeMnNi high-entropy alloy, *Acta Materialia* 61 (2013) 5743.
- [17] W.H. Liu, Y. Wu, J.Y. He, T.G. Nieh, Z.P. Lu, Grain growth and the Hall–Petch relationship in a high-entropy FeCrNiCoMn alloy, *Scripta Materialia* 68 (2013) 526.
- [18] B. Gludovatz, A. Hohenwarter, D. Catoor, E.H. Chang, E.P. George, R.O. Ritchie, A fracture-resistant high-entropy alloy for cryogenic applications, *Science* 345 (2014) 1153.
- [19] M.-H. Tsai, J.-W. Yeh, High-Entropy Alloys: A Critical Review, *Materials Research Letters* 2 (2014) 107.

- [20] B. Gludovatz, E.P. George, R.O. Ritchie, Processing, Microstructure and Mechanical Properties of the CrMnFeCoNi High-Entropy Alloy, *JOM* 67 (2015) 2262.
- [21] O.N. Senkov, S.L. Semiatin, Microstructure and properties of a refractory high-entropy alloy after cold working, *Journal of Alloys and Compounds* 649 (2015) 1110.
- [22] J.P. Couzinié, L. Lilensten, Y. Champion, G. Dirras, L. Perrière, I. Guillot, On the room temperature deformation mechanisms of a TiZrHfNbTa refractory high-entropy alloy, *Materials Science and Engineering: A* 645 (2015) 255.
- [23] G. Dirras, J. Gubicza, A. Heczal, L. Lilensten, J.P. Couzinié, L. Perrière, I. Guillot, A. Hocini, Microstructural investigation of plastically deformed $Ti_{20}Zr_{20}Hf_{20}Nb_{20}Ta_{20}$ high entropy alloy by X-ray diffraction and transmission electron microscopy, *Materials Characterization* 108 (2015) 1.
- [24] G. Laplanche, U.F. Volkert, G. Eggeler, E.P. George, Oxidation Behavior of the CrMnFeCoNi High-Entropy Alloy, *Oxidation of Metals* 85 (2016) 629.
- [25] N.L. Okamoto, S. Fujimoto, Y. Kambara, M. Kawamura, Z.M. Chen, H. Matsunoshita, K. Tanaka, H. Inui, E.P. George, Size effect, critical resolved shear stress, stacking fault energy, and solid solution strengthening in the CrMnFeCoNi high-entropy alloy, *Scientific reports* 6 (2016) 35863.
- [26] N.L. Okamoto, K. Yuge, K. Tanaka, H. Inui, E.P. George, Atomic displacement in the CrMnFeCoNi high-entropy alloy—A scaling factor to predict solid solution strengthening, *AIP Advances* 6 (2016) 125008.
- [27] E.J. Pickering, N.G. Jones, High-entropy alloys: a critical assessment of their founding principles and future prospects, *International Materials Reviews* 61 (2016) 183.
- [28] H.S. Oh, D. Ma, G.P. Leyson, B. Grabowski, E.S. Park, F. Körmann, D. Raabe, Lattice Distortions in the FeCoNiCrMn High Entropy Alloy Studied by Theory and Experiment, *Entropy* 18 (2016) 321.
- [29] G. Laplanche, A. Kostka, C. Reinhart, J. Hunfeld, G. Eggeler, E. George, Reasons for the superior mechanical properties of medium-entropy CrCoNi compared to high-entropy CrMnFeCoNi, *Acta Materialia* 128 (2017) 292.
- [30] K.V. Thurston, B. Gludovatz, A. Hohenwarter, G. Laplanche, E.P. George, R.O. Ritchie, Effect of temperature on the fatigue-crack growth behavior of the high-entropy alloy CrMnFeCoNi, *Intermetallics* 88 (2017) 65.
- [31] D. Miracle, O. Senkov, A critical review of high entropy alloys and related concepts, *Acta Materialia* 122 (2017) 448.
- [32] B. Cantor, I.T.H. Chang, P. Knight, A.J.B. Vincent, Microstructural development in equiatomic multicomponent alloys, *Materials Science and Engineering: A* 375–377 (2004) 213.
- [33] S. Patinet, L. Proville, Depinning transition for a screw dislocation in a model solid solution, *Physical Review B* 78 (2008) 104109.
- [34] L. Proville, S. Patinet, Atomic-scale models for hardening in fcc solid solutions, *Physical Review B* 82 (2010) 054115.
- [35] G. Leyson, L. Hector, W. Curtin, Solute strengthening from first principles and application to aluminum alloys, *Acta Materialia* 60 (2012) 3873.

- [36] G. Leyson, L. Hector, W. Curtin, First-principles prediction of yield stress for basal slip in Mg–Al alloys, *Acta Materialia* 60 (2012) 5197.
- [37] M. Ghazisaeidi, L. Hector, W. Curtin, Solute strengthening of twinning dislocations in Mg alloys, *Acta Materialia* 80 (2014) 278.
- [38] G. Leyson, W. Curtin, Solute strengthening at high temperatures, *Modelling and Simulation in Materials Science and Engineering* 24 (2016) 065005.
- [39] C. Varvenne, A. Luque, W.A. Curtin, Theory of strengthening in fcc high entropy alloys, *Acta Materialia* 118 (2016) 164.
- [40] C. Varvenne, G. Leyson, M. Ghazisaeidi, W. Curtin, Solute strengthening in random alloys, *Acta Materialia* 124 (2017) 660.
- [41] T.M. Smith, M.S. Hooshmand, B.D. Esser, F. Otto, D.W. McComb, E.P. George, M. Ghazisaeidi, M.J. Mills, Atomic-scale characterization and modeling of 60° dislocations in a high-entropy alloy, *Acta Materialia* 110 (2016) 352.
- [42] C. Varvenne, W.A. Curtin, Strengthening of high entropy alloys by dilute solute additions: CoCrFeNiAl_x and CoCrFeNiMnAl_x alloys, *Scripta Materialia* 138 (2017) 92.
- [43] G. Laplanche, O. Horst, F. Otto, G. Eggeler, E.P. George, Microstructural evolution of a CoCrFeMnNi high-entropy alloy after swaging and annealing, *Journal of Alloys and Compounds* 647 (2015) 548.
- [44] F. Otto, N.L. Hanold, E.P. George, Microstructural evolution after thermomechanical processing in an equiatomic, single-phase CoCrFeMnNi high-entropy alloy with special focus on twin boundaries, *Intermetallics* 54 (2014) 39.
- [45] P. Spätig, J. Bonneville, J.L. Martin, A new method for activation volume measurements: application to Ni₃(Al,Hf), *Materials Science Engineering: A* 167 (1993) 73.
- [46] F. Guiu, P.L. Pratt, Stress relaxation and the plastic deformation of solids, *Physica Status Solidi* 6 (1964) 11.
- [47] G. Laplanche, J. Bonneville, A. Joulain, V. Gauthier-Brunet, S. Dubois, Plasticity of the ω-Al₇Cu₂Fe phase, *Journal of Alloys and Compounds* 665 (2016) 144.
- [48] P. Groh, R. Conte, Stress relaxation and creep in α-iron filamentary single crystals at low temperature, *Acta metallurgica* 19 (1971) 895.
- [49] P. Spätig, J. Bonneville, J. Martin, A new interpretation of stress relaxations in Ni₃(Al, Hf) single crystals, *Materials Research Society Symposium Proceedings* 364 (1995) 713.
- [50] Z. Wu, H. Bei, G.M. Pharr, E.P. George, Temperature dependence of the mechanical properties of equiatomic solid solution alloys with face-centered cubic crystal structures, *Acta Materialia* 81 (2014) 428.
- [51] T. Tabata, K. Takagi, H. Fujita, The Effect of Grain Size and Deformation Substructure on Mechanical Properties of Polycrystalline Copper and Cu–Al Alloys, *Transactions of the Japan Institute of Metals* 16 (1975) 569.
- [52] J. Friedel, *Dislocations*, 1st English, Pergamon, Oxford, 1964.
- [53] R. Madec, B. Devincre, L. Kubin, T. Hoc, D. Rodney, The role of collinear interaction in dislocation-induced hardening, *Science* 301 (2003) 1879.
- [54] A. Haglund, M. Koehler, D. Catoor, E.P. George, V. Keppens, Polycrystalline elastic moduli of a high-entropy alloy at cryogenic temperatures, *Intermetallics* 58 (2015) 62.

- [55] G. Laplanche, P. Gadaud, O. Horst, F. Otto, G. Eggeler, E.P. George, Temperature dependencies of the elastic moduli and thermal expansion coefficient of an equiatomic, single-phase CoCrFeMnNi high-entropy alloy, *Journal of Alloys and Compounds* 623 (2015) 348.
- [56] S.I. Hong, J. Moon, S.K. Hong, H.S. Kim, Thermally activated deformation and the rate controlling mechanism in CoCrFeMnNi high entropy alloy, *Materials Science and Engineering: A* 682 (2017) 569.
- [57] Z. Wu, Y. Gao, H. Bei, Thermal activation mechanisms and Labusch-type strengthening analysis for a family of high-entropy and equiatomic solid-solution alloys, *Acta Materialia* 120 (2016) 108.
- [58] C. Davies, V. Sagar, R. Stevens, The effect of stacking fault energy on the plastic deformation of polycrystalline Ni-Co alloys, *Acta Metallurgica* 21 (1973) 1343.
- [59] N. Clement, P. Coulomb, Energies de défaut d'empilement et mécanismes de déformation dans les alliages nickel-chrome, *Philosophical Magazine* 30 (1974) 663.
- [60] N. Clement, D. Caillard, J. Martin, Heterogeneous deformation of concentrated Ni-Cr FCC alloys: Macroscopic and microscopic behaviour, *Acta Metallurgica* 32 (1984) 961.
- [61] J.T.M. De Hosson, G. Boom, U. Schlagowski, O. Kanert, Solution hardening in Al- Zn alloys mean jump distance and activation length of moving dislocations, *Acta Metallurgica* 34 (1986) 1571.
- [62] L. Hollang, E. Hieckmann, D. Brunner, C. Holste, W. Skrotzki, Scaling effects in the plasticity of nickel, *Materials Science and Engineering: A* 424 (2006) 138.
- [63] M. Komarasamy, N. Kumar, R.S. Mishra, P.K. Liaw, Anomalies in the deformation mechanism and kinetics of coarse-grained high entropy alloy, *Materials Science and Engineering: A* 654 (2016) 256.
- [64] H. Mecking, U.F. Kocks, Kinetics of flow and strain-hardening, *Acta Metallurgica* 29 (1981) 1865.

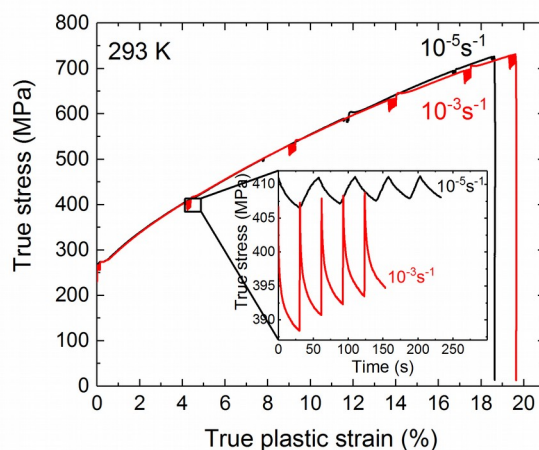


Figure 1: Representative room-temperature stress-strain curves showing negligible effect of strain rate on the flow curves of the CrMnFeCoNi high-entropy alloy. Repeated load relaxation tests (duration 30 s each) were performed at various applied stresses along the true stress-strain curves. The magnified inset shows two such sets performed at comparable flow stresses ($\sim 407\text{--}410$ MPa) at strain rates of 10^{-3} s^{-1} (red curve) and 10^{-5} s^{-1} (black curve).

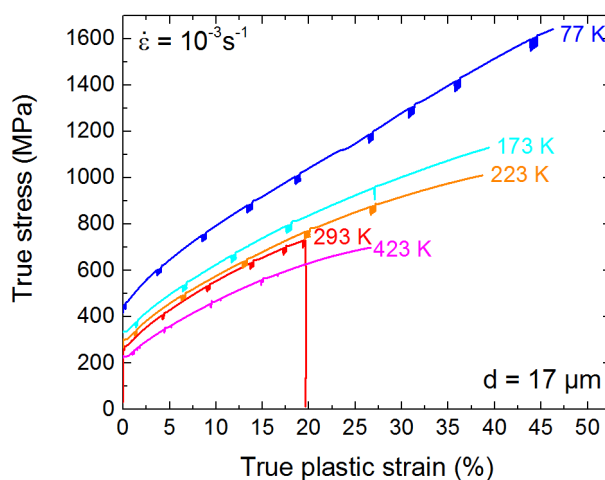


Figure 2: Tensile stress-strain curves of the CrMnFeCoNi high-entropy alloy at various temperatures ranging from 77 K to 423 K.

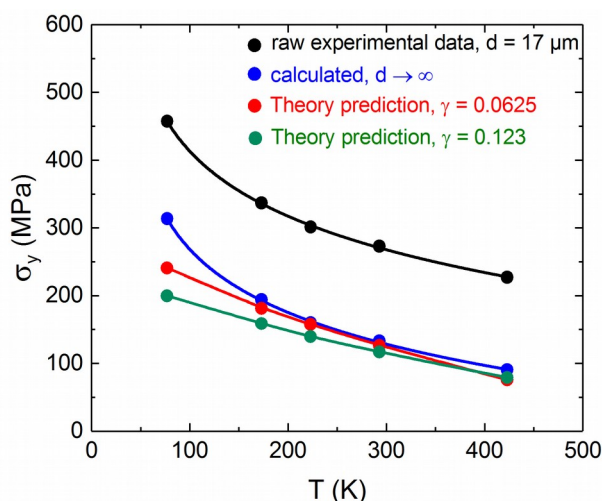


Figure 3: Yield stress σ_y as a function of temperature T . Black data points represent experimental results obtained here for a CrMnFeCoNi HEA with a mean grain size $d = 17 \mu\text{m}$. Blue points are calculated yield stresses for an infinite grain size using the Hall-Petch parameters reported by Otto et al. [16], and thus reflect the lattice strength including solid solution strengthening. Green and red points were calculated using the solid solution strengthening model discussed in section 3 for line tension parameters $\gamma = 0.123$ and 0.0625 , respectively.

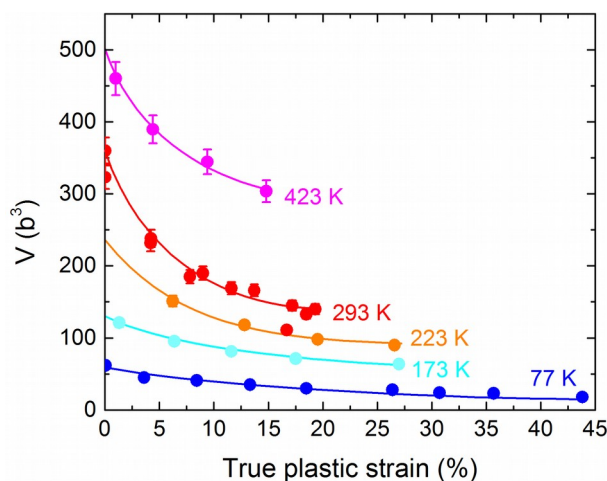


Figure 4: Physical activation volume, obtained at different temperatures, as a function of the true plastic strain. The error bars represent the experimental scatter at 293 K, $\pm 5\%$, obtained from tests performed at two different strain rates (Fig. 1); the same scatter is assumed for the remaining temperatures.

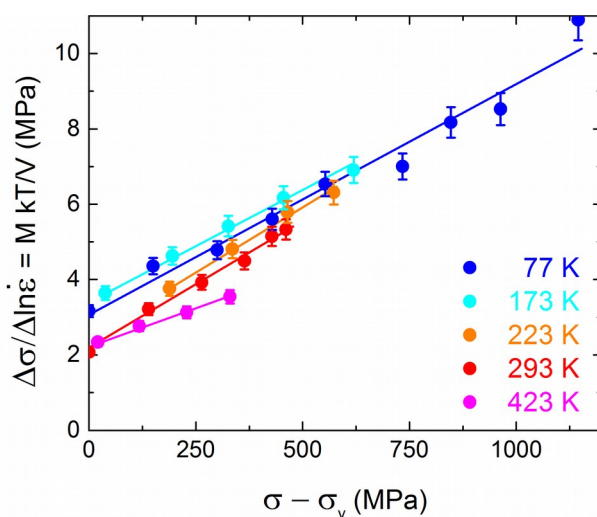


Figure 5: “Haasen plot”, $M k T / V$ versus the offset flow stress $\sigma - \sigma_y$. showing a positive offset at zero indicative of solute strengthening and linear increase with stress indicative of forest hardening.

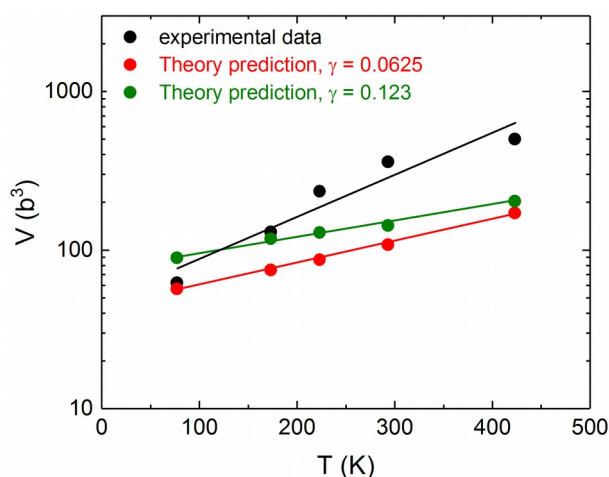


Figure 6: Initial activation volume V determined at the yield stress (in units of b^3) versus temperature. Black symbols are experimental data while green and red symbols were calculated using the solid solution strengthening model developed in section 3 for line tension parameters $\gamma = 0.123$ and 0.0625 , respectively.